Research Article Vol. 6, No. 6 / June 2019 / Optica 805

Imaging with flat optics: metalenses or diffractive lenses?

Sourangsu Banerji,[1] Monjurul Meem,[1] Apratim Majumder,[1] Fernando Guevara Vasquez,[2] Berardi Sensale-Rodriguez,[1] and Rajesh Menon[1,3,*]

[1]Department of Electrical and Computer Engineering, University of Utah, Salt Lake City, Utah 84112, USA
[2]Department of Mathematics, University of Utah, Salt Lake City, Utah 84112, USA
[3]Oblate Optics, Inc. 13060 Brixton Place, San Diego, California 92130, USA
*Corresponding author: rmenon@eng.utah.edu

Received 8 February 2019; revised 14 May 2019; accepted 17 May 2019 (Doc. ID 359356); published 10 June 2019

Recently, there has been an explosion of interest in metalenses for imaging. The interest is primarily based on their subwavelength thicknesses. Diffractive gratings have been used as thin optical elements since the late 19th century. Here, we show that multilevel diffractive lenses (MDLs), when designed properly, can exceed the performance of metalenses. Furthermore, MDLs can be designed and fabricated with larger constituent features, making them accessible to low-cost, large-area volume manufacturing, which is generally challenging for metalenses. The support substrate will dominate overall thickness for all flat optics. Therefore, the advantage of a slight decrease in thickness (from $\sim 2\lambda$ to $\sim \lambda/2$) afforded by metalenses may not be useful. We further elaborate on the differences between these approaches and clarify that metalenses have unique advantages when manipulating the electromagnetic fields, rather than intensity.

https://doi.org/10.1364/OPTICA.6.000805

1. INTRODUCTION

Lenses are fundamental to imaging systems. Conventional lenses exploit refraction to focus light [1]. As a result, a fundamental trade-off increases the thickness and weight of optics with an increasing numerical aperture (or resolution). As illustrated in Fig. 1(a) with the example of a simple planoconvex lens, larger bending angles require larger thicknesses. Recently, there has been significant interest in reducing the thickness and weight of lenses by exploiting diffraction. In such "flat lenses," focusing is achieved by spatially arranging "zones" that impart an appropriate phase to achieve constructive interference of the transmitted waves at the focus [2,3]. As illustrated in Fig. 1(b), larger bending angles may be achieved with no change in thickness, simply by decreasing the local period of the diffractive structure. To ensure constructive interference, each ray must be locally phase shifted to compensate for the variation in its total optical path length to the focus. In traditional diffractive lenses, this is achieved by engineering the path traversed by the ray within the diffractive lens itself, as illustrated in Fig. 1(c). In comparison to traveling the same distance in air, the optical path delay for a thickness, t, is $\Delta = (n-1)\ t$, which then corresponds to a phase shift of $\Delta/\lambda * 2\pi$, where n is the refractive index of the material and λ is the wavelength of light. To achieve a phase shift of 2π, t must be at least $\lambda/(n-1) \sim 2\lambda$ for $n = 1.5$. It is noted that diffractive lenses with numerical aperture (NA) > 1 under water immersion were demonstrated more than a decade ago [4].

To increase the focusing efficiency, blazed or multilevel diffractive lenses (MDLs) were also developed to approximate the optimal continuous phase distribution [see Fig. 1(d)]. In fact, it was widely recognized that close to 100% efficiency could be achieved with such blazed diffractive optics [5]. However, at high numerical apertures, there is a rapid drop in efficiency due to the resonance conditions [6,7]. It was also quite definitively shown that this drop could be avoided by parametric optimization of the geometry of the constituent structures of the diffractive lens using both simulations [7,8] and experiments [9,10]. Another Achilles heel for diffractive lenses has been their poor broadband performance, which was overcome for discrete wavelengths via harmonic phase shifts [11] and by using higher orders of diffraction [12]. We extended this work to continuous broadband spectra using efficient numerical techniques [13–17] and multilevel microfabrication [18] at visible [19–23], longwave infrared (LWIR) [17] and terahertz spectral bands [16,24]. Here, we combine this multilevel approach with parametric optimization to show that high efficiency at a high numerical aperture is indeed feasible for both narrowband and broadband operation, which we believe has not been clearly demonstrated before. We emphasize that MDLs can be fabricated not only in polymers but also in any material that can be etched or deposited (like silicon, glass, etc.). Multilevel microfabrication for MDLs either via single-step grayscale lithography or via multistep lithography and etch process is relatively straightforward due to the larger feature sizes [18]. In summary, MDLs offer a tremendous advantage in manufacturing

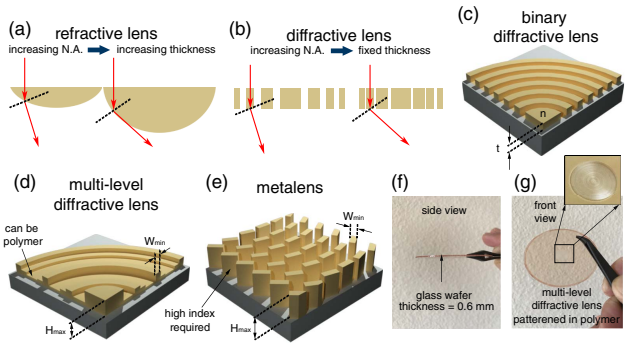

Fig. 1. Bending of light via (a) refraction and (b) diffraction. Schematic of the constituent element of a (c) conventional binary diffractive lens or grating, (d) multilevel diffractive lens (MDL), and (e) metalens. Photographs of a broadband visible MDL fabricated in a polymer film on a glass substrate are shown in (f) side view emphasizing the small thickness, which is dominated by the substrate and (g) front view.

simplicity compared to metalenses with no compromise in performance and no constraints on materials that can be used.

Recently, metalenses were proposed as a means to reduce the overall thickness of the conventional diffractive lens to subwavelength regimes by exploiting magnified phase changes that can occur in resonators [25–32]. Rather than using a traversed path to create a phase shift, appropriately designed subwavelength antenna elements could achieve the same effect [see Fig. 1(e)]. In this paper, we show that the advantages of metalenses might be vastly overstated and that the decrease in thickness from $\sim 2\lambda$ achievable via MDLs to less than λ may not be useful for the majority of applications. To emphasize this point, we show a photograph from the side view [Fig. 1(f)] of a multilevel diffractive lens that is corrected for the visible spectrum. The achromatic MDL depicted in Fig. 1(g) [22,23] was patterned in a photoresist (Microchem, S1813) film atop a glass wafer (thickness ~ 0.6 mm) using grayscale laser patterning with a Heidelberg Instruments MicroPG101 tool. The exposure dose was varied with respect to position to achieve the multiple height levels dictated by the design. Full details of the fabrication process and experimental imaging using similar MDLs are described in [21–23]. We point out that the support substrate will dominate the overall thickness in all cases, and thereby obviate any advantage due to reduction in the device thickness.

We further make the case that MDLs can achieve the same or better optical performance when compared to metalenses. To illustrate this point, we first performed an exhaustive literature survey of metalenses that have been reported so far. A summary of this survey is included in Supplement 1. Then, we selected exemplary metalenses that operate in the narrowband and in the broadband spectral regimes at low, medium, and high numerical apertures, and we designed MDLs having the same optical specifications (focal length, numerical aperture, and operating wavelengths). Finally, we compared the focusing efficiencies of the MDLs to those of the corresponding metalenses. Table 1 summarizes the key results. The first three columns are the optical specifications. Comparing the focusing efficiencies in columns 6 and 9 confirm that MDLs indeed perform better than metalenses. For the MDLs, we used a commonly available polymer photoresist (S1813, Microchem) as the constituent material, since it exhibits high transmission in most wavelength regimes of interest here (measured dispersion is included in Supplement 1), and we have previously fabricated several MDLs in this material [19–23]. In all cases, we assume unpolarized input light for the MDLs.

Third, we point out that the fabrication complexity of metalenses is far higher than that for the MDLs. As can be seen in Table 1 (columns 4 and 7), the minimum feature widths required for metalenses are significantly smaller than those for MDLs. In addition, metalenses generally require high-index materials (see Tables S1 and S2 in Supplement 1), whereas MDLs can be fabricated in low-index polymers. It is important to appreciate that any transparent material can be used for the MDL. This allows MDLs to be mass manufactured at low cost via high-volume imprinting techniques [33].

From a more fundamental standpoint, the problem of designing a lens is related to inverse scattering. Indeed, one can consider two parallel planes: a "lens" plane and a "focal" plane. Then, the goal is to design a lens-field pattern that when illuminated produces a desired focal-field pattern. In the case of monochromatic illumination, where the amplitude and phase of the complex field are both specified in the focal plane (i.e., the focal-field pattern), a lens-field pattern can be simply found using backpropagation. This is an ill-posed problem since there are many lens-field patterns that give approximately the same focal-field pattern (e.g., by adding to the lens-field pattern spatial modes corresponding to evanescent waves). Furthermore, the finite size of the image sensor in the focal plane can also cause ambiguities in the lens-field pattern that depend nonlinearly on the position on the lens plane [34]. In the vast majority of imaging applications, one is interested only in the intensity (amplitude squared) of the focal-field pattern. In this situation, one can readily show by backpropagation that the lens-field pattern is not unique. In the case of broadband illumination, one can expect the solution to this inverse scattering problem to be even more ill posed. This categorically points to the fact that the choice of an ideal phase function for a lens is not necessarily unique. As a result, we argue that optimization is better suited to choose the lens-field pattern.

2. RESULTS AND DISCUSSION

Our design methodology involves nonlinear optimization to select the heights of the constituent elements of the MDL in order to maximize focusing efficiency averaged over all wavelengths of interest as described previously [16,17,21–23]. In congruence with work in metalenses, we define focusing efficiency as the ratio of the power within a spot of diameter equal to 3 times the simulated full width at half-maximum (FWHM) to the total incident power [26]. The point-spread function of each MDL was simulated using the finite-difference time-domain (FDTD) method with the incident electric field polarized in the plane of the MDL. Averaging the fields over the two orthogonal polarization directions of the electric field simulates the point-spread function (PSF) under unpolarized light. All analysis in the main text utilized this PSF assuming unpolarized input. In the FDTD simulations of the MDL, the entire region from the back surface of the lens up to 1.5 times the distance from the focal plane with perfectly-matched-layer boundary conditions was considered. A full 3D FDTD simulation was carried out. To speed up the computation, appropriate symmetry conditions were employed

Table 1. Summary of Performance of MDL and Metalens for Same Optical Specifications[a]

Narrowband			MultiLevel Diffractive Lens			Metalens		
N.A.	Focal Length (μm)	λ (nm)	W_{min} (μm)	H_{max} (μm)	Efficiency (%)	W_{min} (nm)	H_{max} (nm)	Efficiency (%)
0.2	67	530	1	1.1	93	50	600	92 [28]
0.6	200	532	0.4	1.1	90	250	600	87 [29]
0.97	25	1550	0.75	3.1	87	200	950	72 [26]
Broadband			**Multilevel Diffractive Lens**			**Metalens**		
N.A.	Focal Length (μm)	λ	W_{min} (μm)	H_{max} (μm)	Efficiency (%)	W_{min} (nm)	H_{max} (μm)	Efficiency (%)
0.2	63	470–670 nm	1	2	81	80	600	50 [30]
0.36	155	3–5 μm	4	10	86	400	2	70 [31]
0.81	2	560–800 nm	0.35	1.6	70	55	488	69 [32]

[a]Note that W_{min} and H_{max} are defined in Figs. 1(d) and 1(e) for MDL and metalens, respectively.

across the computation region. The mesh accuracy in the FDTD software was $\sim\lambda/20$ [16]. Full details of our simulation are described in Supplement 1. FDTD models for verifying optimized diffractive lenses [13,35] and for simulating high-numerical-aperture zone plates in air [36,37] and under water immersion (with NA > 1) [4] have been reported previously. We note that not all papers follow a consistent method for calculating focusing efficiency. Therefore, we have included a brief description of the methods used in select metalens papers in Supplement 1.

A. Narrowband MDLs

First, we consider the design of MDLs for discrete wavelengths (narrowband). Following the parameters from Table 1, we designed three MDLs with (focal length, numerical aperture) = (67 μm, 0.2), (200 μm, 0.6), and (25 μm, 0.97), respectively.

The optimized designs represented by the height distribution of the concentric rings are illustrated in Figs. 2(a), 2(c), and 2(e) for NA = 0.2, 0.6, and 0.97 MDLs, respectively. The corresponding simulated PSFs are shown in Figs. 2(b), 2(d), and 2(f), respectively. The FWHM noted in the insets of the PSFs confirm close to diffraction-limited performance. The simulations confirm that even at an NA as high as 0.97 efficiencies more than 87% is maintained, superior to those of the corresponding metalenses (Table 1). We note that shadowing effects can clearly affect focusing efficiencies at high NA for both metalenses and MDLs. Our simulations simply point out that metalenses do not offer any advantage over MDLs for narrowband operation, while exhibiting equivalent optical performance.

B. Broadband MDLs

One of the big advantages of MDLs as we have pointed out before is their good achromatic performance over broad spectral bands [17,21–24]. Here, we reiterate this claim by directly comparing MDLs with metalenses of the same optical specifications. Again, following the parameters from Table 1, we designed three broadband MDLs with (focal length, numerical aperture) = (63 μm, 0.2), (200 μm, 0.36) and (2 μm, 0.81). The optimized designs represented by the height distribution of the concentric rings are illustrated in Figs. 3(a)–3(c) for NA = 0.2, 0.36, and 0.81 MDLs, respectively. The corresponding simulated point-spread functions (PSFs) for three representative wavelengths are shown in Figs. 3(d), 3(g), and 3(j); 3(e), 3(h), and 3(k); 3(f), 3(i), and 3(l), respectively. Again, the FWHM noted in the insets of the PSFs confirm close to diffraction-limited performance for all wavelengths. The simulations confirm that even at NA as high as 0.81 efficiencies of 70% are maintained across the entire band, which are superior to those of the corresponding metalenses (Table 1).

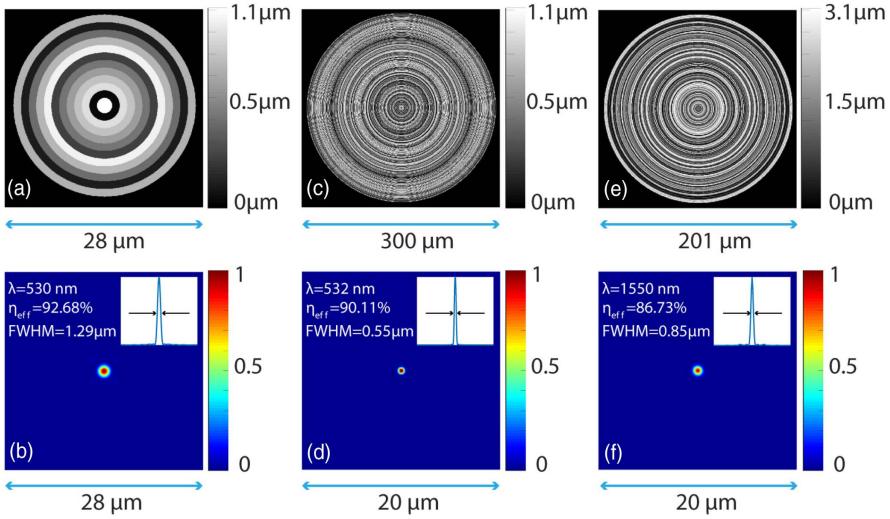

Fig. 2. Narrowband MDLs. Designed-height distribution (top row) and simulated point-spread function (bottom row) for (a) and (b) low, (c) and (d) medium, and (e) and (f) high-NA MDLs are shown.

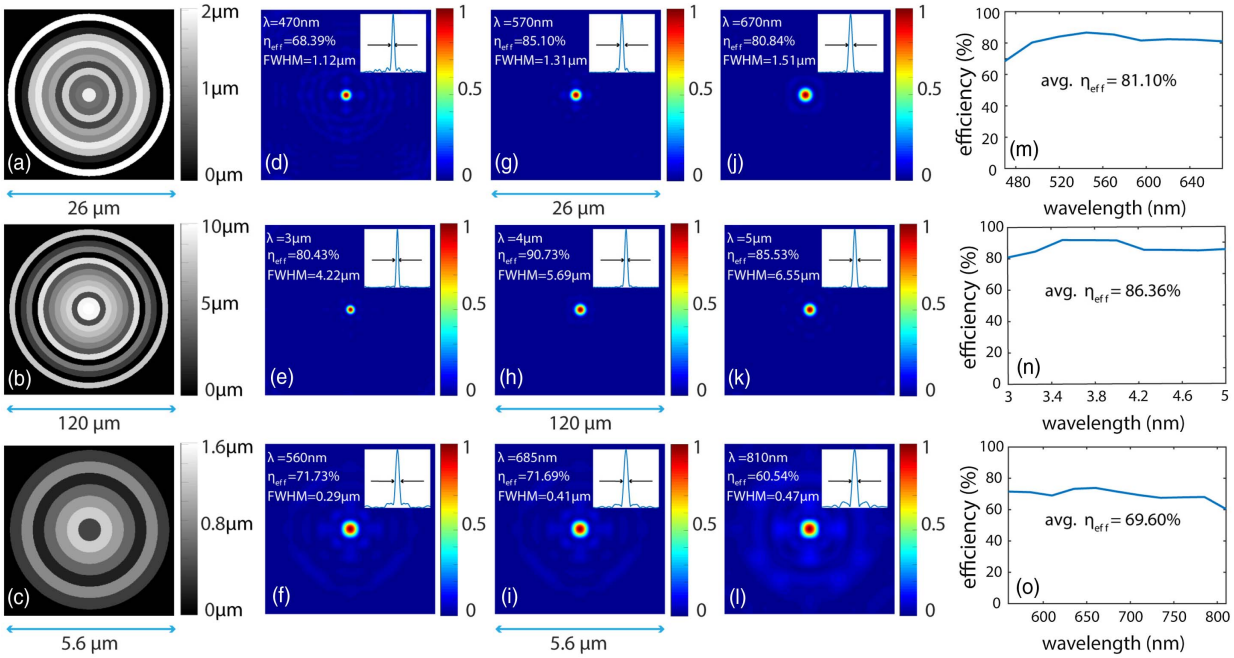

Fig. 3. Broadband MDLs. (a)–(c) Designed-height distributions, (d)–(l) simulated point-spread functions, and (m)–(o) simulated focusing efficiency spectra for low-, medium-, and high-NA MDLs.

3. ABERRATIONS ANALYSIS

When illuminated by a normally incident uniform plane wave, an ideal lens will generate a perfectly spherical wavefront that converges to the ideal focus. Aberrations in an actual lens are defined as the difference between the actual wavefront from this ideal wavefront. Here, we use the simulated wavefront to analyze the aberrations that are present in MDLs. Using the Zernike-polynomial representation of aberrations, we can calculate the wavefront errors as illustrated in Fig. 4 for the broadband MDL with on-axis PSFs at NA = 0.81, $f = 2$ μm computed at $\lambda = 560$ nm. Similar results for the other lenses as well as details of the aberrations analysis are included in Supplement 1.

Furthermore, Table 2 summarizes the Zernike coefficients (in units of wavelengths) for the narrowband on-axis MDL with NA = 0.97, $f = 25$ μm, and $\lambda = 1550$ nm, and the broadband on-axis MDL with NA = 0.81 and $f = 2$ μm, simulated at representative wavelengths of $\lambda = 560$ nm, 685 nm, and 810 nm, respectively. These calculations confirm that MDLs have extremely low aberrations and the broadband MDLs exhibit very low variation in aberrations across the operating wavelength range. In addition, we performed simulations for one broadband MDL (NA = 0.81, $f = 2$ μm) to demonstrate that the depth of focus is comparable to that of a conventional lens (see Supplement 1) across a broad spectrum. We also performed FDTD simulations

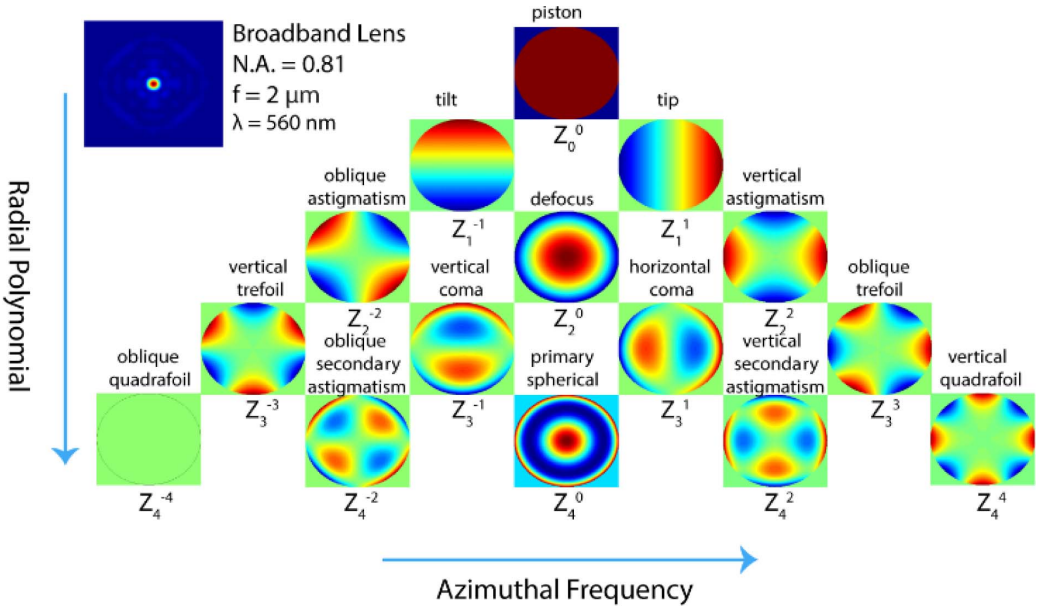

Fig. 4. Aberrations analysis in form of Zernike polynomials for NA = 0.81, $f = 2$ μm MDL simulated at $\lambda = 560$ nm.

Table 2. Zernike Coefficients (in Units of λ) for Two Exemplary High-NA MDLs; One Narrowband and Another Broadband

Multilevel Diffractive Lens [Narrowband (N.A. = 0.97)]										
λ	Piston	Tip	Tilt	Defocus	Vertical Astigmatism	Oblique Astigmatism	Vertical Coma	Horizontal Coma	Oblique Trefoil	Vertical Trefoil
1550 nm	3.53E − 5	−6.89E − 22	−1.77E − 22	−8.78E − 5	5.78E − 21	1.56E − 22	7.21E − 22	6.07E − 22	1.36E − 4	4.66E − 22
Multilevel Diffractive Lens (Broadband (N.A. = 0.81))										
λ	Piston	Tip	Tilt	Defocus	Vertical Astigmatism	Oblique Astigmatism	Vertical Coma	Horizontal Coma	Oblique Trefoil	Vertical Trefoil
560 nm	1.85E − 2	1.84E − 19	−6.75E − 20	−2.47E − 2	3.10E − 19	8.26E − 20	2.04E − 19	−9.55E − 20	4.06E − 2	1.65E − 18
685 nm	2.16E − 2	−5.61E − 19	−2.08E − 20	−3.26E − 2	2.97E − 18	7.66E − 20	7.65E − 19	−1.18E − 19	3.18E − 2	1.38E − 18
810 nm	4.23E − 2	−4.21E − 19	4.96E − 20	−4.56E − 2	2.68E − 18	6.08E − 20	1.90E − 18	2.11E − 19	2.21E − 2	3.57E − 18

of the off-axis PSFs showing good performance (see Supplement 1) also at a broad spectrum. We emphasize that experimental imaging with broadband MDLs have already been demonstrated in the visible [22,23] and in the LWIR bands [17].

A. Where Are Metaoptics Useful?

Finally, we would also like to clarify the regimes where metaoptics (which includes metamaterials, metasurfaces, and metalenses) have distinct advantages over MDLs and conventional diffractive optics. Metaoptics have the advantage of extreme form birefringence, which enables them to manipulate the polarization states of light in unique manners. A few illustrative examples of these advantages have already been demonstrated in polarimetric imaging [38], high-efficiency polarizers [39], and polarization-sensitive optics [40]. Additionally, their subwavelength dimensions are extremely useful in integrated optics and photonics, where density is a critical parameter for technology adoption [41–43]. We surmise that metaoptics is useful when manipulating electromagnetic fields. In conventional imaging, it is the intensity (square of the field) that is important. Therefore, MDLs are sufficient and far easier to fabricate.

4. CONCLUSION

Using a series of rigorous simulations, we conclude that multilevel diffractive lenses, when designed appropriately, can provide better optical performance, while being significantly simpler to manufacture, when compared to metalenses. MDLs can exploit the relatively mature mass manufacturing capabilities that exist in the hologram industry to create low-cost, large-area flat optics, enabling a new era of ultralightweight, thin optical systems.

Funding. Office of Naval Research (ONR) (N66001-10-1-4065); National Science Foundation (NSF) (ECCS #1351389).

Acknowledgment. We thank Tom Tiwald from Woollam for assistance with dispersion measurements.

See Supplement 1 for supporting content.

REFERENCES

1. M. Born and E. Wolf, *Principle of Optics*, 7th ed. (Cambridge University, 1999).
2. D. Gil, R. Menon, and H. I. Smith, "The case for diffractive optics in maskless lithography," J. Vac. Sci. Technol. B **21**, 2810–2814 (2003).
3. D. A. Buralli and G. M. Morris, "Design of diffractive singlets for monochromatic imaging," Appl. Opt. **30**, 2151–2158 (1991).
4. D. Chao, A. A. Patel, T. Barwicz, H. I. Smith, and R. Menon, "Immersion zone-plate-array lithography," J. Vac. Sci. Technol. B **23**, 2657–2661 (2005).
5. M. B. Fleming and M. C. Hutley, "Blazed diffractive optics," Appl. Opt. **36**, 4635–4643 (1997).
6. R. Petit, ed., *Electromagnetic Theory of Gratings* (Springer, 1980).
7. E. Noponen, J. Turunen, and A. Vasara, "Parametric optimization of multilevel diffractive optical elements by electromagnetic theory," Appl. Opt. **31**, 5910–5912 (1992).
8. E. Noponen, J. Turunen, and A. Vasara, "Electromagnetic theory and design of diffractive-lens arrays," J. Opt. Soc. Am. A **10**, 434–443 (1993).
9. J. M. Finlan, K. M. Flood, and R. J. Bojko, "Efficient f:1 binary-optics microlenses in fused silica designed using vector diffraction theory," Opt. Eng. **34**, 3560–3564 (1995).
10. T. Shiono, T. Hamamoto, and K. Takahara, "High-efficiency blazed-diffractive optical elements for the violet wavelength fabricated by electron-beam lithography," Appl. Opt. **41**, 2390–2393 (2002).

11. D. W. Sweeney and G. E. Sommargren, "Harmonic diffractive lenses," Appl. Opt. **34**, 2469–2475 (1995).
12. D. Faklis and G. M. Morris, "Spectral properties of multiorder diffractive lenses," Appl. Opt. **34**, 2462–2468 (1995).
13. R. Menon, P. Rogge, and H. Y. Tsai, "Design of diffractive lenses that generate optical nulls without phase singularities," J. Opt. Soc. Am. A **26**, 297–304 (2009).
14. G. Kim, J. A. Dominguez-Caballero, and R. Menon, "Design and analysis of multi-wavelength diffractive optics," Opt. Express **20**, 2814–2823 (2012).
15. R. Menon and P. Wang, "Nanophotonic scattering structure," U.S. patent 8,953,239 (10 February 2015).
16. S. Banerji and B. Sensale-Rodriguez, "A computational design framework for efficient, fabrication error-tolerant, planar THz diffractive optical elements," Sci. Rep. **9**, 5801 (2019).
17. M. Meem, S. Banerji, A. Majumder, F. G. Vasquez, B. Sensale-Rodriguez, and R. Menon, "Broadband lightweight flat lenses for long-wave-infrared imaging," arXiv:1904.09011 (2019).
18. G. J. Swanson, "Binary optics technology: the theory and design of multi-level diffractive optical elements," Technical Report 854 (MIT Lincoln Laboratory, 1989).
19. N. Mohammad, M. Meem, X. Wan, and R. Menon, "Full-color, large area, transmissive holograms enabled by multi-level diffractive optics," Sci. Rep. **7**, 5789 (2017).
20. G. Kim, J. A. Dominguez-Caballero, H. Lee, D. Friedman, and R. Menon, "Increased photovoltaic power output via diffractive spectrum separation," Phys. Rev. Lett. **110**, 123901 (2013).
21. P. Wang, N. Mohammad, and R. Menon, "Chromatic-aberration-corrected diffractive lenses for ultra-broadband focusing," Sci. Rep. **6**, 21545 (2016).
22. N. Mohammad, M. Meem, B. Shen, P. Wang, and R. Menon, "Broadband imaging with one planar diffractive lens," Sci. Rep. **8**, 2799 (2018).
23. M. Meem, A. Majumder, and R. Menon, "Full-color video and still imaging using two flat lenses," Opt. Express **26**, 26866–26871 (2018).
24. S. Banerji, A. Chanana, H. Condori, A. Nahata, and B. Sensale-Rodriguez, "Efficient design of diffractive THz lenses for aberration rectified focusing via modified binary search algorithm conference on lasers and electro-optics," in *Conference on Lasers and Electro-Optics*, OSA Technical Digest (online) (2018), paper JW2A.76
25. N. Yu, P. Genevet, M. A. Kats, F. Aieta, J. P. Tetienne, F. Capasso, and Z. Gaburro, "Light propagation with phase discontinuities: generalized laws of reflection and refraction," Science **334**, 333–337 (2011).
26. A. Arbabi, Y. Horie, A. J. Ball, M. Bagheri, and A. Faraon, "Subwavelength-thick lenses with high numerical apertures and large efficiency based on high-contrast transmitarrays," Nat. Commun. **6**, 7069 (2015).
27. P. Lalanne and P. Chavel, "Metalenses at visible wavelengths: past, present, perspectives," Laser Photon. Rev. **11**, 1600295 (2017).
28. W. T. Chen, A. Y. Zhu, J. Sisler, Z. Bharwani, and F. Capasso, "A broadband achromatic polarization-insensitive metalens consisting of anisotropic nanostructures," arXiv:1810.05050 (2018).
29. F. Aieta, P. Genevet, M. A. Kats, N. Yu, R. Blanchard, Z. Gaburro, and F. Capasso, "Polarization insensitive metalenses at visible wavelengths," Nano Lett. **12**, 4932–4936 (2012).
30. W. T. Chen, A. Y. Zhu, V. Sanjeev, M. Khorasaninejad, Z. Shi, E. Lee, and F. Capasso, "A broadband achromatic metalens for focusing and imaging in the visible," Nat. Nanotechnol. **13**, 220–226 (2018).
31. S. Zhang, A. Soibel, S. A. Keo, D. Wilson, B. Rafol, D. Z. Ting, A. She, S. D. Gunapala, and F. Capasso, "Solid-immersion metalenses for infrared focal-plane arrays," Appl. Phys. Lett. **113**, 111104 (2018).
32. Y. Liang, H. Liu, F. Wang, H. Meng, J. Guo, J. Li, and Z. Wei, "High-efficiency, near-diffraction limited, dielectric metasurface lenses based on crystalline titanium dioxide at visible wavelengths," Nanomaterials **8**, 288 (2018).
33. U. Palfinger, L. Kuna, D. Nees, S. Ruttloff, J. Götz, and B. Stadlober, "R2R fabrication of freeform micro-optics," Proc. SPIE **10520**, 105200J (2018).
34. S. Maretske, "Locality estimates for Fresnel-wave-propagation and instability of x-ray phase contrast imaging with finite detectors," arXiv:1805.06185 (2018).
35. X. Wan, B. Shen, and R. Menon, "Diffractive lens design for optimized focusing," J. Opt. Soc. Am. A **31**, BB27–BB33 (2014).
36. R. Menon, D. Gil, and H. I. Smith, "Experimental characterization of focusing by high-numerical-aperture zone plates," J. Opt. Soc. Am. A **23**, 567–571 (2006).
37. D. Gil, R. Menon, and H. I. Smith, "Fabrication of high-numerical aperture phase zone plates with a single lithography exposure and no etching," J. Vac. Sci. Technol. B **21**, 2956–2960 (2003).
38. M. Khorasaninejad, W. T. Chen, A. Y. Zhu, J. Oh, R. C. Devlin, D. Rousso, and F. Capasso, "Multispectral chiral imaging with a metalens," Nano Lett. **16**, 4595–4600 (2016).
39. B. Shen, P. Wang, R. C. Polson, and R. Menon, "An ultra-high efficiency metamaterial polarizer," Optica **1**, 356–360 (2014).
40. E. Arbabi, S. M. Kamali, A. Arbabi, and A. Faraon, "Full-stokes imaging polarimetry using dielectric metasurfaces," ACS Photon. **5**, 3132–3140 (2018).
41. B. Shen, P. Wang, R. C. Polson, and R. Menon, "An integrated-nanophotonic polarization beamsplitter with 2.4 μm × 2.4 μm2 footprint," Nat. Photonics **9**, 378–382 (2015).
42. B. Shen, R. C. Polson, and R. Menon, "Increasing the density of integrated-photonic circuits via nanophotonic cloaking," Nat. Commun. **7**, 13126 (2016).
43. A. Majumder, B. Shen, R. C. Polson, and R. Menon, "Ultra-compact polarization rotation in integrated silicon photonics using digital metamaterials," Opt. Express **25**, 19721–19731 (2017).